41st European Rotorcraft Forum

UNSTEADY ACTUATING BLADE MODEL FOR CFD/CSD ANALYSIS OF A TILTROTOR

M. Valentini*, G. Droandi*, P. Masarati*, G. Quaranta*

*Dipartimento di Scienze e Tecnologie Aerospaziali – Politecnico di Milano
Campus Bovisa, Via La Masa 34, 20156 Milano – Italy
e-mail: mirco.valentini@polimi.it

Abstract

The paper presents an effective method to evaluate the unsteady flow field around a rotor through a Computational Fluid Dynamics model based on the actuator blade approach. The actuator blade extends the classical actuator disk model without the necessity to perform time or azimuth averaging operations. In this way, a time accurate investigation of the influence of the rotor wake on the rotor itself and on other non-rotating parts (fuselage, wings) can be performed. The method exploits the overset grid technique to allow an easy identification of the location of the sources distributed in the flow field to enforce the correct blade loads. The kinematics and the dynamics of the rotating parts is computed thought the coupling with a multibody solver and transmitted to the CFD as movement of the independent surface grids associated with each actuator blade. This allows to keep into account both rigid and elastic movements, including those related to movable surfaces. A comparison with experimental results obtained for a four blade tiltrotor are shown to verify the quality of the prediction of the flow field. Additionally, a comparison with the results obtained through a classical actuator disk allows to quantify the effects of the employment of the time-accurate approach with respect to the time-averaged results of the actuator disk model.

1. INTRODUCTION

The simulation of the flow field around a helicopter or a tiltrotor is a formidable task that still requires a large computational burden to be accomplished. As a consequence simple, inexpensive computational methods, such as vortex methods or the classical blade element momentum (BEM) theory, are still the main design methods, especially when aeroelastic solutions are sought and whenever it is not necessary to analyse the details of the flow field close to the rotor blades. Among these simplified models, the actuator disk (AD) associated with Computational Fluid Dynamics (CFD) simulation has seen a widespread use, see Refs [1].

In this approach, the rotor is represented by an infinitesimally thin disk which introduces a pressure discontinuity based on momentum theory. The effect of the rotor on the flow field could be represented using a source term in the momentum and energy equations or enforcing a pressure jump on the disk boundary. In all cases it is necessary to supply the load distribution on the rotor, and this can be done computing the sectional loads using the blade element theory (BET). This approximation results in a dramatic reduction of

computational workload, and was first introduced by Whitfield and Jameson [2] to study the propeller wing interaction, and in general it can be very useful whenever it is required to investigate the impact of the flow field generated by the rotor and its wake on other bodies, like the airframe or the wings in tiltrotors [3, 4, 5]. Additionally, it is not required to generate complex individual blade conformal grids, reducing significantly the time required for the preparation of the computational model. Of course the AD approach introduces the assumption of time-averaged flow, that for the rotors operating in periodic regime ruled by the passage of each individual blade along the different azimuth positions results in an approximation through an azimuth-averaged representation. Few attempts have been made to extend the idea of AD to the analysis of unsteady flows by means actuator blades models that are able to represent the the discrete blade structure of the rotor, capturing the helical vortex wake created by the rotating blades [6].

This work presents an innovative and efficient method to simulate the flow field around rotating blades extending the classical AD model to the representation of unsteady flow field. The proposed method is based on an actuating blade (AB) model applied in the frame of overset system of moving multi-block grids and was successfully implemented in the CFD code ROSITA (ROtorcraft Software ITAly [7]) developed at Department of Aerospace Science and Technology (DAER) of Politecnico di Milano. In order to properly capture the kinematics of the rotor blades during their motion, the AB model was coupled with a multibody dynamic model. For this purpose, the CFD code ROSITA was weakly coupled with the Computational Structural Dynamics (CSD) code MBDyn (MultiBody Dynamics [8]) developed at DAER. The AB surfaces and the load distributions applied on them were continuously adapted during the simulation in order to reach the prescribed rotor trim state. Consequently, as done in Ref. [9], the source distribution used to enforce the pressure discontinuity caused by the blade passages takes fully into accounts the blade dynamics adapting the geometry during the time marching simulation. At the same time the blade loads where computed in MBDyn using the local flow velocity provided by the CFD.

The reliability of the trimmed AB model and the coupling strategy with MBDyn were demonstrated simulating the flow field around the isolated rotor of a tiltwing aircraft [10] in hover. The rotor kinematics and the flow field predicted by the AB model were first compared with results of calculations performed using the simpler trimmed AD model [9]. Second, the trimmed AB model was validated comparing numerical results with available experimental data [11] on the reference geometry.

2. CFD/CSD SOLVERS

2.1 ROSITA overset CFD solver for rotorcraft

The CFD code ROSITA [7] is a compressible Reynolds Averaged Navier-Stokes (RANS) equations solver coupled with the one-equation turbulence model of Spalart-Allmaras [12]. Multiple moving multi-block grids can be used to form an overset grid system by means of the Chimera technique. The Navier-Stokes equations are formulated in terms of the absolute velocity in an overset system of moving multi-block Cartesian grids. A cell-centred finite-volume implementation of the Roe's scheme [13] is used to discretise in space the equations. Second order accuracy is obtained through the use of MUSCL extrapolation with a modified version of the Van Albada limiter introduced by Venkatakrishnan [14]. The viscous terms are computed by the application of the Gauss theorem and using a cell-centred discretisation scheme. Time advancement is carried out with a dual-time formulation [15], employing a 2^{nd} order backward differentiation formula to approximate the time derivative and a fully unfactored implicit scheme in pseudo-time. The generalised conjugate gradient (GCG), in conjunction with a block incomplete lower-upper preconditioner, is used to solve the resulting linear system.

The connectivity between the (possibly moving) component grids is computed using the Chimera technique. The approach adopted in ROSITA is derived from that originally proposed by Chesshire and Henshaw [16], with modifications to further improve robustness and performance. During the execution of the tagging procedure, the domain boundaries with solid wall conditions are firstly identified and all points in overlapping grids that fall close to these boundaries are marked as holes (seed points). Then, an iterative algorithm identifies the donor and fringe points and lets the hole points grow from the seeds until they entirely fill the regions outside the computational domain. Oct-tree and alternating digital tree data structures are employed in order to speed up the search of donor points.

The ROSITA solver is fully capable of running

in parallel on computing clusters. The parallel algorithm is based on the message passing programming paradigm and the parallelisation strategy consists in distributing the grid blocks among the available processors. Each grid block can be automatically subdivided into smaller blocks by the solver to attain an optimal load balancing.

2.2 MBDyn multibody solver for aeromechanics

MBDyn is an open source general-purpose multibody analysis software developed by the researchers of DAER. It is mainly intended for dynamics simulations, although it provides some intrinsic multidisciplinary analysis capabilities. Even thought it is de facto a general purpose multibody software, it is mildly oriented towards the aeromechanical analysis of rotorcraft systems through the availability of simplified built-in rotor blade BET aerodynamics [17]. The analysis is based on the integration in time of the Newton-Euler equations of motion of a set of discrete bodies, subjected to configuration-dependent forces that model deformability and aerodynamic loads, and connected by kinematic constraints expressed using the Lagrangian multipliers formalism. The deformable components library consists in lumped components, kinematically exact and composite-ready nonlinear beam elements suitable for the modelling of rotor blades, and component mode synthesis elements, mainly used for the modelling of non-rotating components, like the airframe. The modularity of the formulation eased the coupling with the ROSITA CFD solver.

3. ACTUATING BLADE MODEL

The AB model is derived directly from a steady AD model already embedded in ROSITA which reproduces the effects of the rotor blades using a disk having the same diameter of the rotor itself [9].

In particular, the AB model described in this paper is based on the main idea of replacing each rotor blade by a localised actuator surface, allowing to retain the unsteady framework. Rotor blades are projected onto their mean surfaces, ideally infinitely thin –de facto represented as a single layer of cells– which carries discontinuities of flow properties. The pressure jumps created by the rotor blades into the airflow are imposed only in correspondence of the thin surfaces representing the blade projections. The unsteady motion of the rotating system is well reproduced since the actuating surfaces can rotate around the rotor axis. In this way, limitations due to the assumption of time-averaged flow, commonly employed in the classical steady AD models included in CFD codes, are overcome since the flow field around the blades is reproduced in a time-dependent manner. As shown by O'Brien [18], the use of an actuating surface provides also a better resolution of the flow physic with respect to more conventional actuating line models since in the latter case each blade is represented by a single line of sources.

The implementation of the AD model in ROSITA is founded on the addition of source terms to the momentum and energy equations, as explained by Biava et al. [9].

Considering the non-dimensionalised Reynolds Averaged Navier-Stokes equations in integral Arbitrary Lagrangian Eulerian (ALE) form applied to a volume Ω with a surface boundary $\partial\Omega$:

$$\frac{\mathrm{d}}{\mathrm{d}t}\int_{\Omega}\mathbf{u}\mathrm{d}V+\oint_{\partial\Omega}[\mathbf{f}_c(\mathbf{u})-\mathbf{u}\nu]\cdot\mathbf{n}\mathrm{d}A - \oint_{\partial\Omega}\mathbf{f}_d(\mathbf{u},\boldsymbol{\nabla}\mathbf{u})\cdot\mathbf{n}\mathrm{d}A=\int_{\Omega}\mathbf{s}(\mathbf{u})\mathrm{d}V \tag{1}$$

where the vector $\mathbf{u}(\mathbf{x},t)$ stores the unknown conservative variables, i.e. density, momentum and total energy, while vector $\mathbf{f}_c$ includes the inviscid convective flux functions, $\mathbf{f}_d$ includes the diffusive flux terms, $\mathbf{s}$ is the source term and the vector $\nu(t)$ represents the local velocity of all the moving boundaries, due to entrainment and grid deformation, if present.

Source terms are introduced in a single layer of cells of a cylindrical grid which contain the AD. This solution is preferred to other implementation strategies for its robustness as compared to the enforcement of boundary condition on variables [5] or on fluxes [19] as stated by Le Chuiton [1]. Since it is assumed that the actuator blade source layer is fixed in a strip of the structured grid, see figure 6, the source vector $\mathbf{s}$, calling $\mathbf{F}=(F_x,F_y,F_z)^T$ the vector of force per unit area distribution, can be written as

$$\mathbf{s}=\begin{Bmatrix}0\\F_x\\F_y\\F_z\\\mathbf{F}\cdot\frac{(\rho\mathbf{v})^*}{(\rho)*}\end{Bmatrix} \tag{2}$$

where the symbol $(\cdot)^*$ is used to represent the averaged value between those computed above and below the blade source element strip.

The same modelling strategy is used to implement the AB method here presented. However, in this case each rotor blade is represented by a

Cartesian grid containing the blade mean surface. The forces developed by each blade are introduced in the flow filed by means of a non uniform source distribution arranged in a single layer of cells of each blade grid. The Chimera technique allows to correctly place the blade grids in the flow filed. Every time the blade motion is periodic and the rotor kinematics can be prescribed at the very beginning of the simulation, the computational effort could be reduced since the tagging procedure which build the final mesh for each time step can be performed as a one time pre-processing step. On the other hand, if the blade motion is not known a priori, the tagging algorithm must be performed at each time step during the calculation. However, since an AB grid contains a small number of elements, the execution of the tagging algorithm does not significantly increase the computational time required.

4. COUPLING STRATEGY

The AB model will be coupled with a multibody dynamic model of the rotor through a weak CFD/CSD coupling algorithm, in order to capture the correct kinematics of the rotor blades.

The couple CFD/CSD method proceed as follows:

(a) MBDyn computes an initial trim state using one of its embedded simple inflow models and provides the loads history on a rotor revolution. For each blade and for each time step MBDyn provides a one dimensional map which connects the loads distribution and the radial position on the blade.

(b) Loads provided by MBDyn are the interpolated on the actuating balde surface in such a way that the global load on the rotor is conserved. ROSITA is then run until a periodic state condition at the blade surface is reached, thus providing an updated induced velocity history on a rotor revolution to the CSD solver.

(c) Induced velocities porvided by ROSITA, are used by MBDyn to compute a new trimmed solution and to find the updated loads history.

Points (b) and (c) are repeated until the variation of the rotor commands between two successive coupling cycles is below a prescribed tolerance. The coupling method has demonstrated to be able to reach a converged solution within 5-10 cycles.

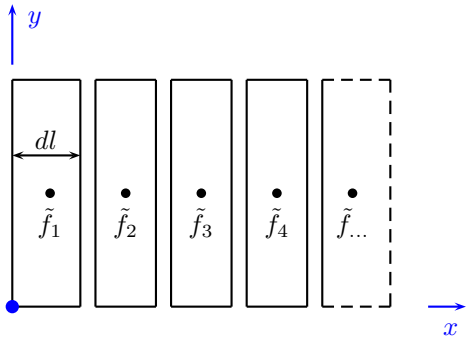

Figure 1: Sketch of the MBDyn BEM grid.

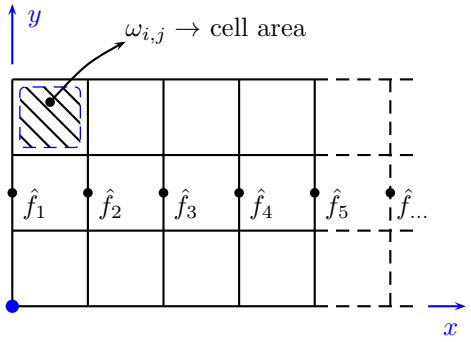

Figure 2: Loads interpolation points on the CFD grid.

4.1 Loads interpolation

In order to map the loads between the CSD and CFD grids, the main assumption we have done is to consider the chords of both grids aligned to the y-axis of the local reference frame in which the grid is described. Thanks to that assumption, the load interpolation can be done along the x-axis of the grids. The first step of the mapping is to compute the loads per unit length provided by MBDyn (see Figure 1). The second stage is to interpolate the force per unit length on the CFD grid (see Figure 2). This operation is done by using a simple linear interpolation, with the forcing of 0 value in extrapolation.

$$\hat{f}_i = \text{interp}\left(\frac{\tilde{f}_i}{dl_i}, \tilde{x}, \hat{x}\right)$$

The next stage is to compute the integral force on each strip of the CFD grid, and this can be done using the trapezoidal rule. Before this step it is also possible to insert a filter in order to smooth the load distribution .

$$\bar{f}_i = 0.5\left(\hat{f}_i + \hat{f}_{i+1}\right)(\hat{x}_{i+1} - \hat{x}_i)$$

The last step is to distribute the loads over the

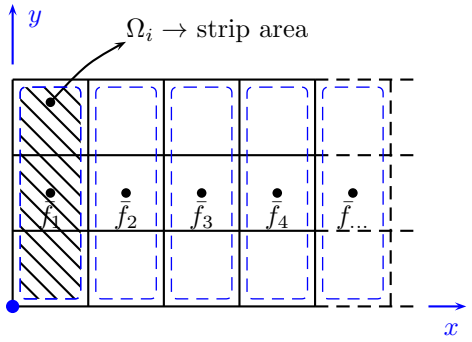

Figure 3: Loads integration scheme on the CFD grid.

chords (as shown in Figure 3). This operation can be done in two ways:

- using only forces
- using moments

In the first case, the load distribution is considered constant on each (chord aligned) strip, and its value is simply:

$$f_{i,j} = \frac{F_i}{\Omega_i} \qquad \forall j$$

In the second case in which the moments are taken into account, the loads distribution in chord is considered linear, and the parameters of the curve are computed in the following manner:

$$\begin{cases} f_{i,j} & = & A_i\, y_{i,j} + B_i \\ \sum_{j=0}^{M} \omega_{i,j} & = & \Omega_i \end{cases}$$

$$\begin{cases} \sum_{j=1}^{M} \left(A_i\, y_{i,j} + B_i\right) \omega_{i,j} & = & \bar{f}_i \\ \sum_{j=1}^{M} \left(A_i\, y_{i,j} + B_i\right) \omega_{i,j}\, y_{i,j} & = & \bar{m}_i^x \end{cases}$$

Where $y_{i,j}$ is the distance between the force application point and the pole of the moment. Using the last two equation it is possible to write a simple 2×2 linear system for each strip to find the load distribution in chord.

$$\begin{bmatrix} \omega_i^T\, \mathbf{y}_i & \omega_i^T\, \mathbf{1} \\ \omega_i^T\, \mathbf{y}_i^2 & \omega_i^T\, \mathbf{y}_i \end{bmatrix} \begin{Bmatrix} A_i \\ B_i \end{Bmatrix} = \begin{Bmatrix} \bar{f}_i \\ \bar{m}_i^x \end{Bmatrix}$$

When the load distribution is computed, it is possible to rescale all the distribution by a constant factor in order to recover the original integral load on the blade.

4.2 Velocity interpolation and relaxation parameter

Induced velocities are extracted from the velocity field by taking the mean value of the velocity on the upper and lower layers with respect to the actuating blade, and the mean value in chord.

MBDyn can perform the interpolation in three different ways:

- One dimensional interpolation for each blade using the radial coordinate, in this case the procedure is the same used for the loads;
- One dimensional interpolation for each blade using the radial coordinate and forcing the mean value between all the blades at the same azimuthal position, even in this case the procedure is the used for the loads, the only difference is that in this way all the blades uses the same induced velocity at the same angular position;
- Two dimensional interpolation from a disk. In this case, velocities are projected on the tip path plane, and then re-interpolated on a equally spaced grid. At this point it is possible to smooth the velocity distribution using a prescribed number of Fourier modes.;

In order to increase the computational stability of the method, it also possible to introduce a relaxation parameter which consider a linear combination of the velocities at the last two cycles.

5. RESULTS AND DISCUSSION

In order to assess the reliability of the coupled unsteady AB model described in this paper, an experimental database gathered at Politecnico di Milano [11] during the tests of a tiltwing tiltrotor aircraft was used. The aircraft was a civil passenger transportation aircraft [10] belonging to the same class of ERICA [20] and was characterised at full-scale by a trapezoidal wing with a span of 15 m and two four-bladed rotors with a radius of 3.7 m.

With the aim of validating the trimmed AB model, only the isolated tiltwing rotor case in hovering condition was considered. Coupled CFD/CSD analyses were performed to prove that the coupling strategy was suitable to correctly compute the trim commands for the rotor in order to satisfy the trim requirements. Moreover, a detailed analysis of the results was carried out to demonstrate the capability of the trimmed AB model to properly predict the unsteady flow field

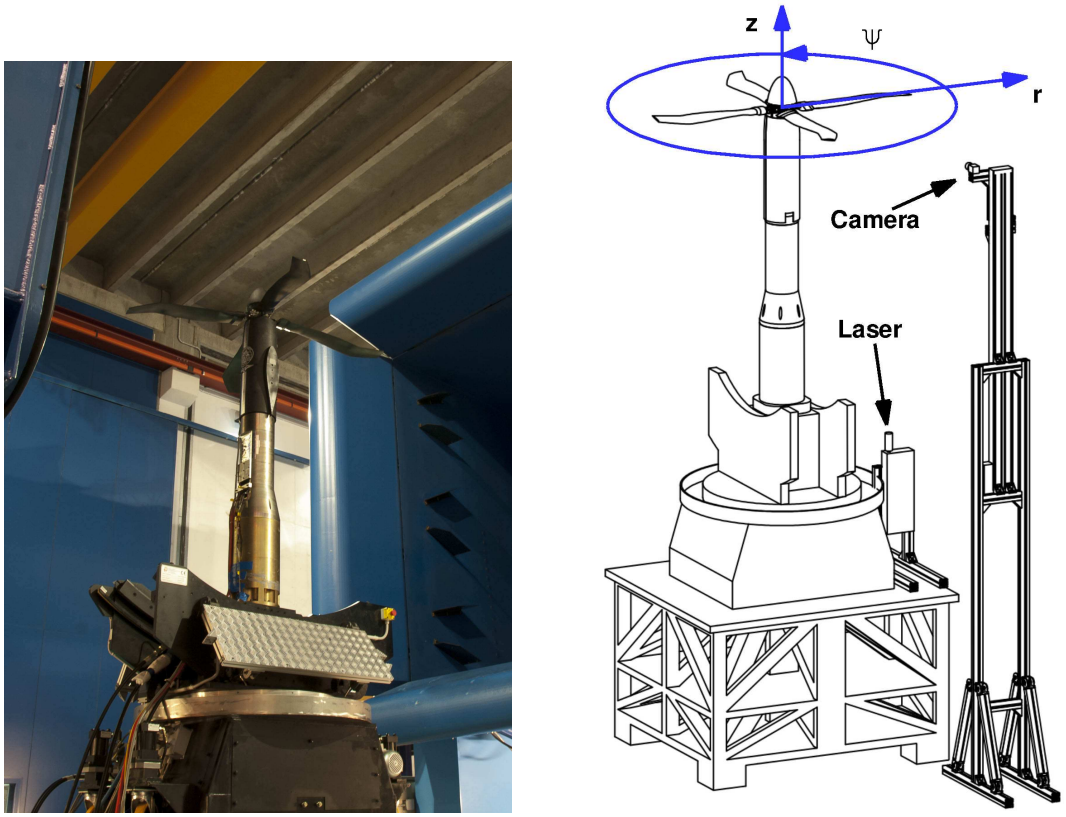

(a) The rotor model in the open test section of the Politecnico di Milano Large Wind Tunnel

(b) Schematic view of the PIV set up

Figure 4: The experimental isolated rotor model.

below the rotor. Calculations were carried out both with the well established trimmed AD model [9] and with the trimmed AB model described in this paper. Rotor kinematics and inflow conditions calculated with the two methods were analysed and compared with available experimental data. Finally, the flow field computed with the unsteady trimmed AB model was compared with PIV data.

5.1 Experimental set up

A wind tunnel model [11, 10, 21] representing the isolated rotor of the considered tiltwing aircraft was realised at the DAER Aerodynamics Laboratory of Politecnico di Milano and was tested in the open test section of the in the Politecnico di Milano Large Wind Tunnel, as shown in Figure 4(a). The experimental test rig essentially consisted of the rotor hub, the four blades designed in-house [22], the rotor pylon and its basement. The tiltwing rotor model had a geometrical scale of 1/4 with respect to the full-scale aircraft, thus the rotor radius was $R = 0.925$ m. During the hovering tests, the tip Mach number was $M_{Tip} = 0.32$ and corresponds to 1/2 the tip Mach number of full-scale aircraft in helicopter mode.

The rotor hub, placed at a height of 5 R from the ground, was powered by a hydraulic motor located in a aluminium basement below a rigid pylon. The thrust given by the rotor was measured by a six-component strain gauge hollow balance located under the rotor hub. The torque was measured by an in-house instrumented hollow shaft which passed through the balance. The carbon fibre nacelle was mounted on the lower part of the rotor pylon. The hub was a typical helicopter rotor hub since it was fully articulated. The collective, longitudinal and lateral pitch controls were provided to the blades by three electric actuators acting on the rotor swashplate. Each blade was attached to the rotor hub through the flap, lead-lag and pitch hinges located in different positions. In particular, the lead-lag hinge was located beyond the flap hinge while the feathering bearing was placed further outboard. No dampers were fitted on the

lead-lag hinge of the rotor model. To directly measure the pitch, lead-lag and flap angles on the rotor hinges, Hall effect sensors were employed on each blade hinge.

An extensive Particle Image Velocimetry (PIV) campaign has been carried out on the model in order to accurately investigate the flow field below the rotor blades. The PIV setup [23] was composed by a Nd:YAG double pulsed laser with 200 mJ output energy and a wavelength of 532 nm and a double shutter CCD camera with a 12 bit, 1952×1112 pixel array. The camera was mounted on a single axis traversing system to move the measurement window in vertical direction. The laser was mounted below the rotor disk to light an (r, z) plane. In particular, an azimuthal measurement plane perpendicular to the rotor disk was considered. A sketch of the PIV set up is shown in Figure 4(b) where also the reference system is illustrated. The measurement area was 0.38 R wide and 0.90 R high. Phase-locked PIV measurements were carried out by synchronising the laser pulses with a prescribed azimuthal position of the rotor blade. The final vector fields were computed by averaging 100 vector fields (coming from image pairs post-processing [24]) for each blade azimuthal position considered.

5.2 Numerical Model

The CFD model of the isolated tiltwing rotor was composed by a total of three to six Cartesian multiblock grids, depending on method chosen to model the rotor (respectively AD and AB). The different grids were mounted together by ROSITA using the Chimera technique. When the AD model was used, the final computational mesh consisted of 2 different background meshes and 1 mesh for the actuator disk. On the other hand, when the AB model was employed, 4 identical meshes that represented the actuating blades were used instead of the actuator disk mesh. Both grid systems are reported in Figure 5. The background mesh was composed by 2 different cylindrical grids containing a total of about 4.17×10^6 cells. A coarse grid (outer grid, of 1.06×10^6 cells) was created to represent the flow domain far from the rotor while a fine grid (inner grid, of 3.11×10^6 cells) was designed to model the flow region close to the blades. The actuator disk grid, shown in Figure 6(a), was a cylindrical grid of 0.20×10^6 cells while the actuating blades, illustrated in Figure 6(b), were modelled with 4 rectangular grids containing 0.13×10^6 cells each.

Since in hovering flight some regions of the flow field showed very low velocities, computations were performed using the Turkel's low Mach number preconditioner [25] and low values of the Courant-Friedrichs-Lewy (CFL) number (equal to 5). When the AD model was employed to reproduce the rotor effects, a steady-state approach was used to perform the calculations. On the contrary, when the AB model was used, CFD simulations were carried out in a time accurate manner and every time step the AB grids were rotated of 2° with respect to the background grids. At the beginning of the first cycle, the simulation was started with an impulsive start of the blades while the other cycles were started using the final flow field solution of the previous cycles (with the updated blade kinematics). In order to reach a fully developed state of the wake system, at least six complete rotor revolutions were needed in the first cycle, while four complete rotor revolutions were required in the following cycles.

The multibody dynamic model of the rotor was realised with MBDyn and represented the fully articulated rotor hub of the wind tunnel model. In particular, the swashplate, the four pitch links, the rotor hinges (flap, lead-leg, pitch) and the four blades were included in the MBDyn model. The blades were considered in the dynamic model as rigid bodies with given mass and inertia properties. The aerodynamic mesh of the each blade, as shown in Figure 7, was composed by a total of 40 strips distributed in a suitable manner along the blade span. MBDyn embedded a simple aerodynamic solver based on the Blade Element Momentum Theory (BEMT) approach. The airfoil aerodynamic characteristics required to the BEMT solver were stored in tables for a wide range of angles of attack, Reynolds and Mach numbers, combining wind tunnel data [26] and two-dimensional CFD results obtained with ROSITA.

When coupled CFD/CSD analyses were performed, the load distribution applied by ROSITA on each actuating surface (AD or AB) at a certain iteration of the coupling procedure was computed by MBDyn using the inflow model derived by ROSITA at the end of the previous iteration. At the very beginning of the trim procedure, MBDyn used the Pitt-Peters [27] inflow model to compute the correct load distribution on the rotor blades and to predict the rotor trim state. The rotor kinematic predicted at every cycle by MBDyn was used at the beginning of every corresponding CFD analysis by ROSITA to correctly move the AD or AB grids toward the updated tip path plane or blades positions.

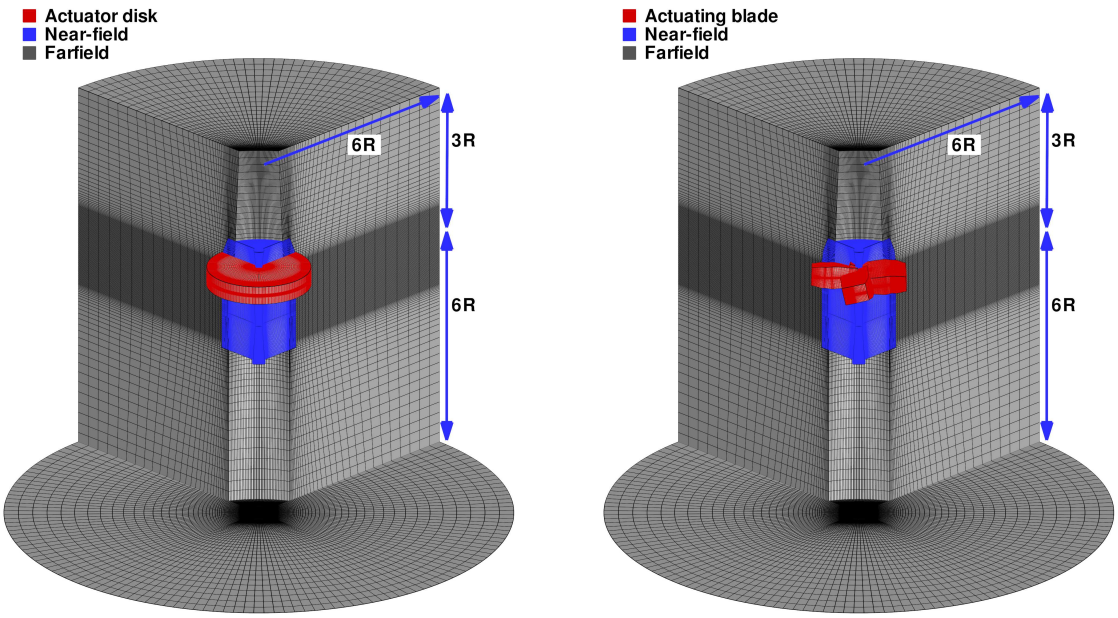

(a) Grid system for the AD model

(b) Grid system for the AB model

Figure 5: CFD grid systems of the isolated rotor.

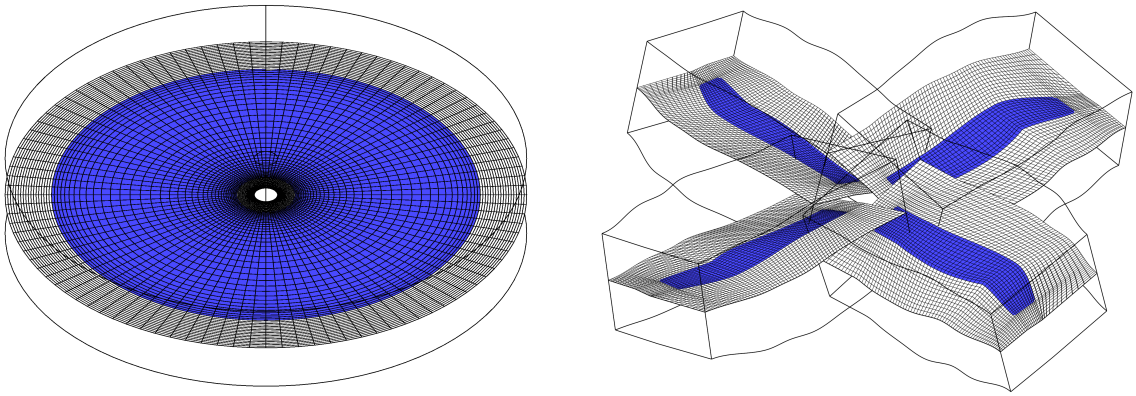

(a) Actuator disk grid

(b) Actuating blades grids

Figure 6: AD and AB grids details (the blue regions correspond to the source layer on the AD or AB region).

5.3 Results

The test case selected from the available experimental database for the validation of the trimmed AB model corresponds to the case of the isolated tiltwing rotor model in hover (shaft angle $\alpha_s = 0°$) with a tip Mach number of 0.32. In such operative condition, a thrust coefficient C_T equal to 0.015 was obtained with a collective angle θ_0 of 12.0° and a coning angle β_0 of 2.6°. This particular condition corresponds to the rotor trim condition used to acquire PIV images in the wake system of the isolated rotor in hover.

Numerical simulations carried out with the trimmed AD model took 9 MBDyn/ROSITA coupling cycles to converge and required a total of about 47 hours. To perform each steady computation, the CFD solver ROSITA was run in parallel on 65 processors. In order to reach a fully developed flow filed state, each simulation was carried out over 2000 pseudo-iterations and took about 5

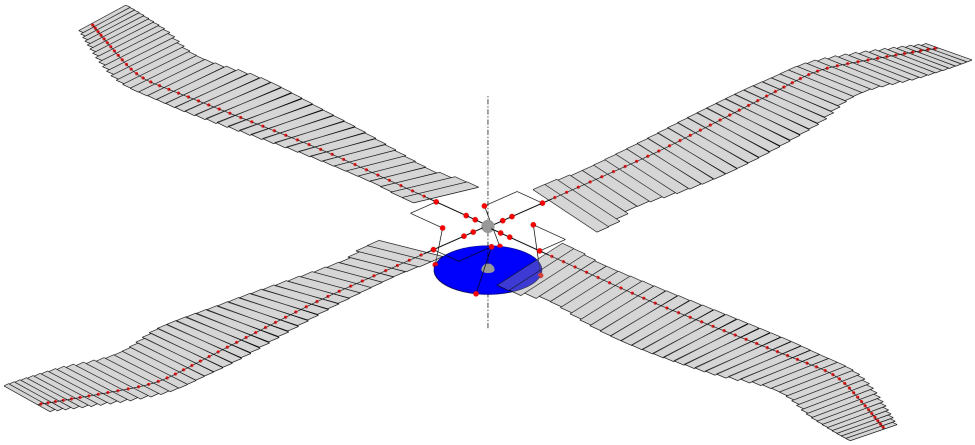

Figure 7: Sketch of the MBDyn multibody dynamic model of the rotor head.

hours (wall clock). At each cycle, MBDyn required about 10 minutes to reach a converged state solution.

When the trimmed AB model was used, only 7 MBDyn/ROSITA coupling cycles were performed in order to find a converged solution. Nevertheless, in the AB model the unsteady nature of the CFD calculations leads to a substantial increase of the computational time of the whole simulation (about 224 hours) with respect to the simpler AD model. To speed up the calculations, the CFD solver ROSITA was run in parallel on 128 processors (twice the number of processors employed in the AD case). A complete rotor revolution was performed in 180 real time steps (for each real time step ROSITA performed 80 pseudo-iterations) and was accomplished in about 7 hours. During the first coupling cycle 6 rotor revolutions were needed to reach a fully developed state of the wake system taking about 42 hours. The successive cycles were carried out over 4 rotor revolutions taking about 28 hours each. At the beginning of each CFD calculation the rotor blade kinematics was known a priori over a complete rotor revolution as it was predicted by the CSD solver. As consequence, the tagging procedure can be performed in advance on the nested Chimera grid system by ROSITA for a single rotor revolution and stored to be retrieved during the actual calculation. This feature allows to strongly reduce the computational cost of each CFD run and, thanks to the limited number of elements of each blade grid, represents a valid alternative to the method proposed by Lynch et all. [6] which is based on the KD-tree search algorithm. However, when numerical simulations were performed, the tagging procedure cannot be performed in parallel in the coupled CFD/CDS framework, thus the it took about 2 hours for each cycle.

The rotor blade kinematics were reported in Figure 8 where the acquired experimental values of pitch (θ_0) and coning (β_0) angles are compared with the those predicted by the two numerical approaches. The hinge angles computed with both methods converged toward the same values even though their evolution over the iteration cycles present some differences. In particular, the pitch angle predicted with the trimmed AB model exhibits a slower convergence with respect to the one obtained with the trimmed AD model. This different behaviour is mainly due to the different values of the relaxation parameter used in MBDyn to stabilise the calculations and to guarantee good convergence properties (note that a lower relaxation parameter was used for AB case). A good agreement between computed and measured data is apparent both for the pitch and for the coning angles (see Figure 8(a) and 8(b)).

The analysis of the power coefficient (C_P) evolution over the iteration cycles shows that the coupled AD and AB models tend to converge toward slightly different solutions. Moreover, as illustrated in Figure 9, both methods underestimated the power coefficient measured in the experiment. However, numerical results demonstrated that the AB model allows to better predict the rotor power coefficient as it results closer to the experimental data (at last iteration the difference is about 9.0 %) with respect to the one found with the AD model (that shows a difference of 14.5 %). This result is a direct consequence of the rotor inflow computed by ROSITA and exploited by MBDyn to predict the rotor trim state and its performance. Indeed,

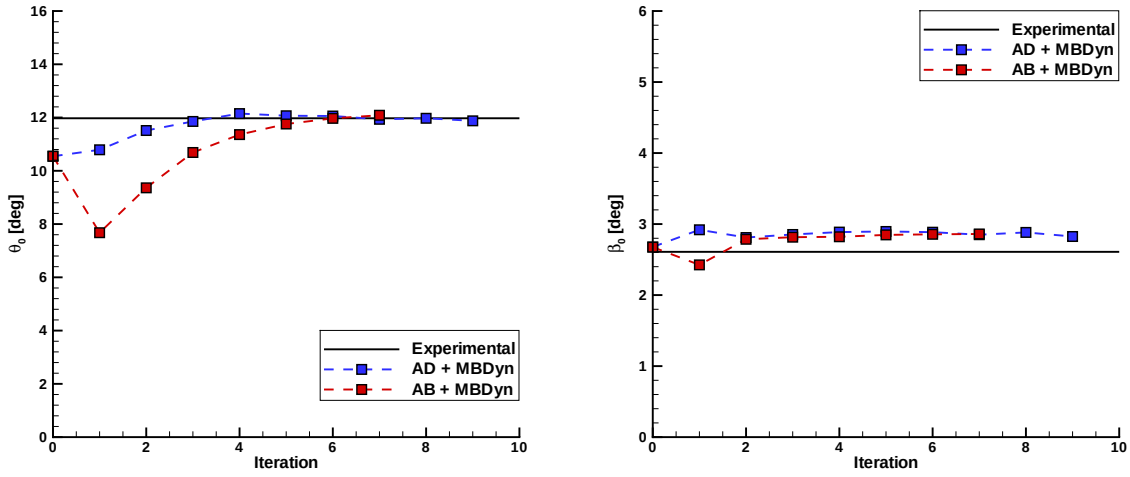

(a) Pitch angle

(b) Flap angle

Figure 8: Kinematic parameters evolution over the iteration cycles: comparison between measured data [10] and computed values of the hinge angles.

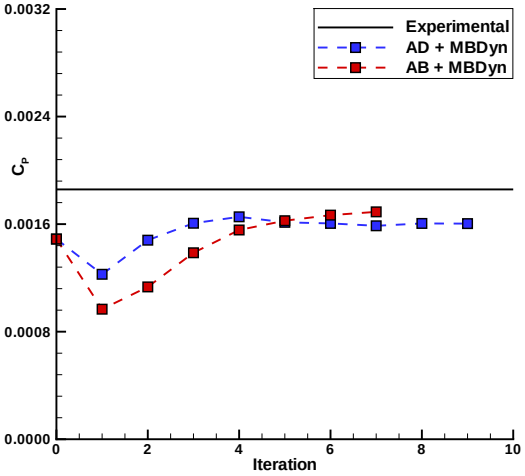

Figure 9: Power coefficient evolution over the iteration cycles: comparison between measured [10] and computed values.

the unsteady behaviour of the rotor wake directly influences the rotor inflow and thus its kinematics and its performance. The AB model can correctly represent the unsteady flow field around the rotating blades since the method is able to describe the evolution of the rotor wake (blade tip vortex) in a time dependent manner. It follows that at the end of each unsteady calculation, the resulting inflow model includes all the unsteady effects due to the blade passage over different azimuthal positions. On the other hand, under the assumption of time-averaged flow, steady CFD calculations carried out with the classical AD model can reproduce only the mean effects of the rotor on the flow field. The inflow models produced in this way contained only an averaged representation of the effects given by the blades rotation. As consequence, this approximation leads to a worse estimation on the rotor performance (C_P). Figure 10 shows the axial velocity distribution (U_z) on a z-constant plane just below the rotor. The figure highlights the differences between the velocity distribution obtained under a time-averaged approximation (Figure 10(a)) and with an unsteady calculation (Figure 10(b)). A localised increase of the axial velocity in the region close to the blades' trailing edge (especially at the tip) underlines the rotor blades passage in the velocity field of Figure 10(b). The AD is not able to capture this effect and the resulting field in this case shows an axisymmetric distribution of the axial velocity U_z (see Figure 10(a)). Even though the instantaneous velocity fields obtained with the AB model are strongly influenced by the actual position of the blades, the radial distribution of the azimuth-averaged axial velocity profile (computed over the final rotor revolution) shows a behaviour similar to the mean velocity profile given by the AD model, as illustrated in Figure 11. Moreover, comparing the mean velocity profiles extracted for each coupling cycle, it can be observed that in both cases the velocity profiles converged toward a similar distribution after 3 cycles.

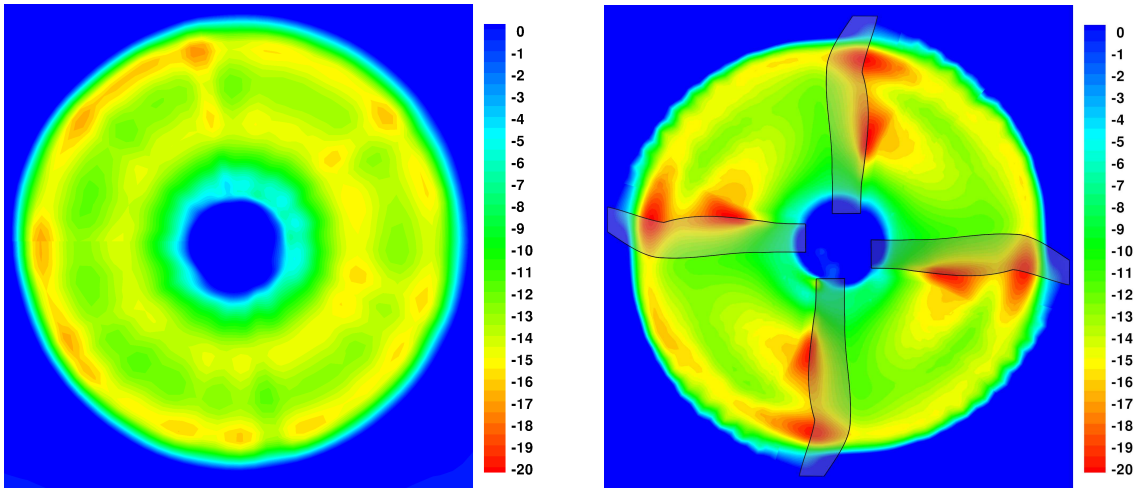

(a) Actuator disk (Iteration 8)

(b) Actuating blade, last real time step (Iteration 6)

Figure 10: Axial velocity distribution on a plane at $z/R = -0.015$ (top view).

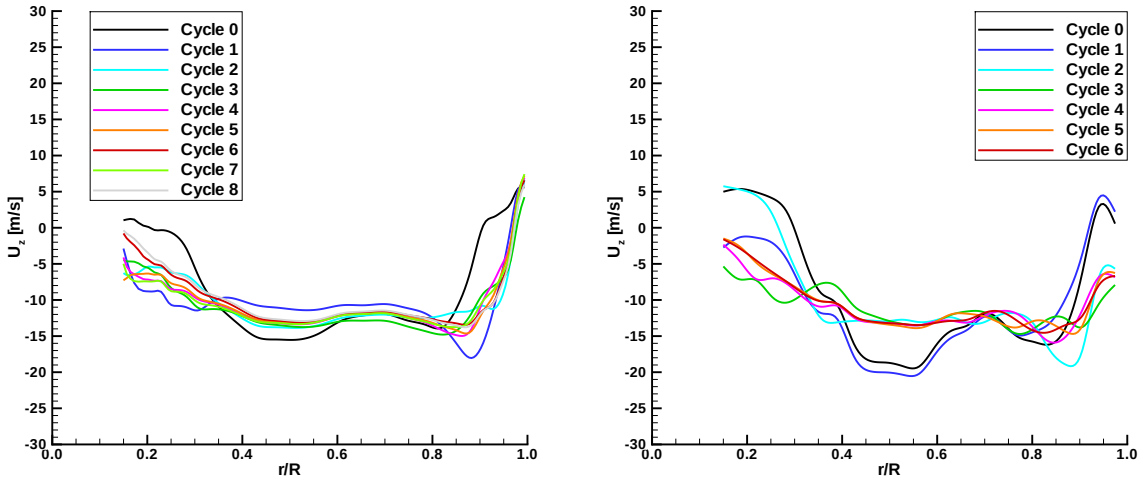

(a) Actuator disk

(b) Actuating blade

Figure 11: Radial distribution of axial velocity component U_z over the iteration cycles.

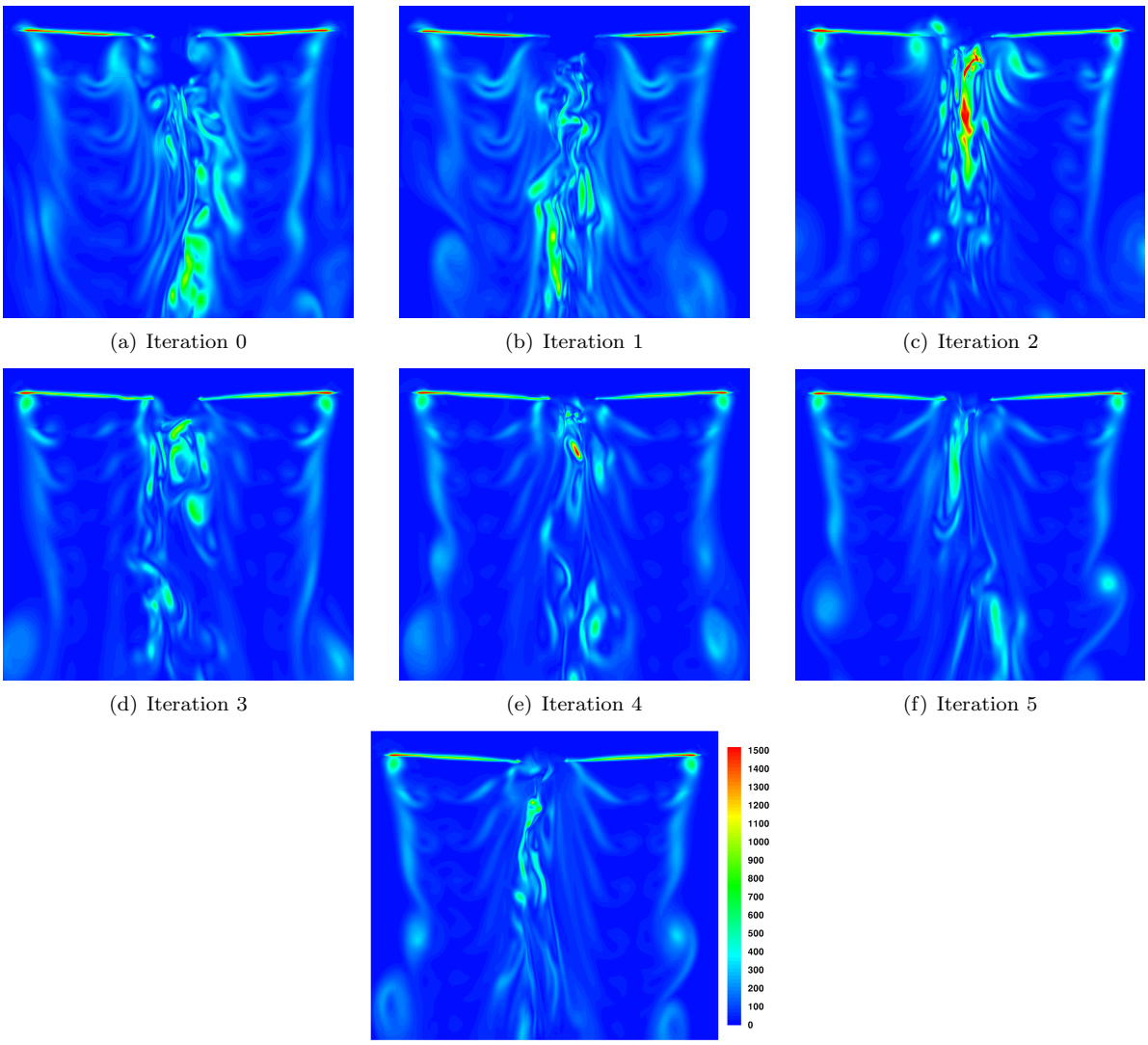

(a) Iteration 0 (b) Iteration 1 (c) Iteration 2

(d) Iteration 3 (e) Iteration 4 (f) Iteration 5

(g) Iteration 6

Figure 12: Flow field comparison over the iteration cycles for the AB model coupled with MBDyn: contours of the vorticity magnitude in an azimuthal plane at $\psi = 0°$ (flow field solution are extracted from the final time step of each unsteady computation).

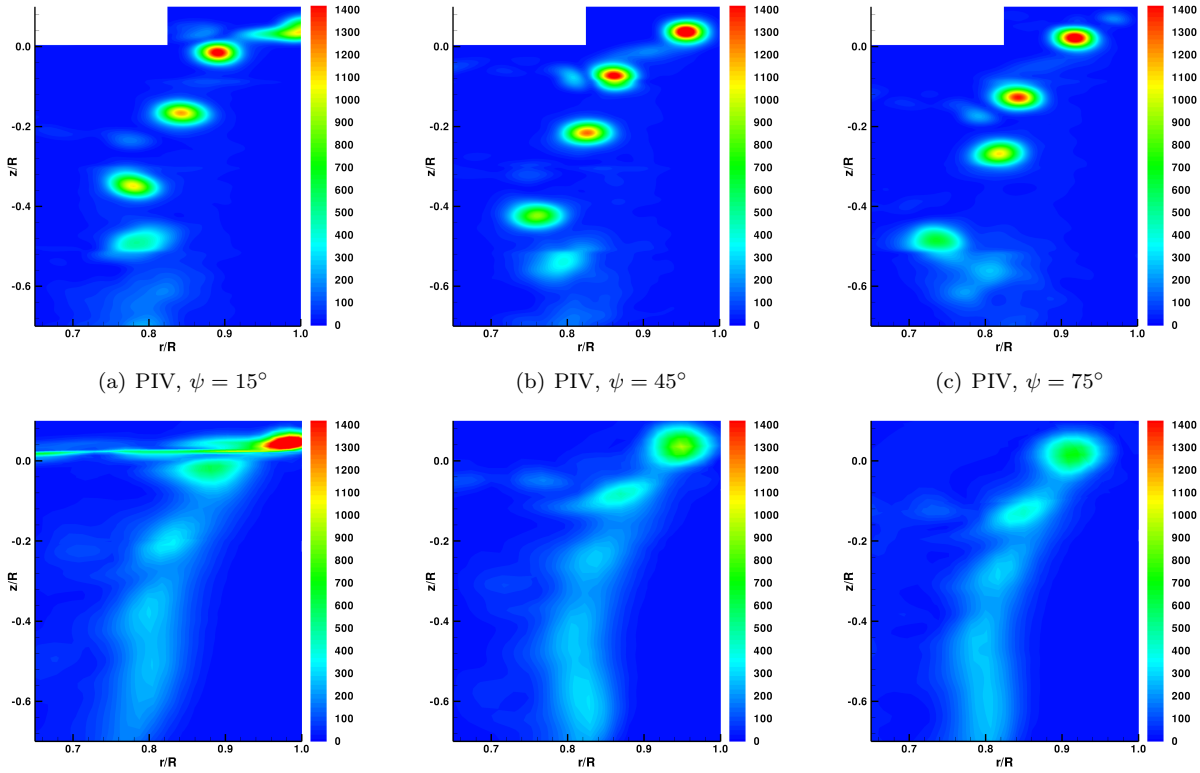

(a) PIV, $\psi = 15°$ (b) PIV, $\psi = 45°$ (c) PIV, $\psi = 75°$

(d) CFD, $\psi = 15°$ (e) CFD, $\psi = 45°$ (f) CFD, $\psi = 75°$

Figure 13: Vorticity magnitude contours in an azimuthal plane: comparison between PIV measurements [11] and unsteady CFD calculations performed using the AB model. CFD results are extracted from the final time step of the final coupling iteration (cycle 6).

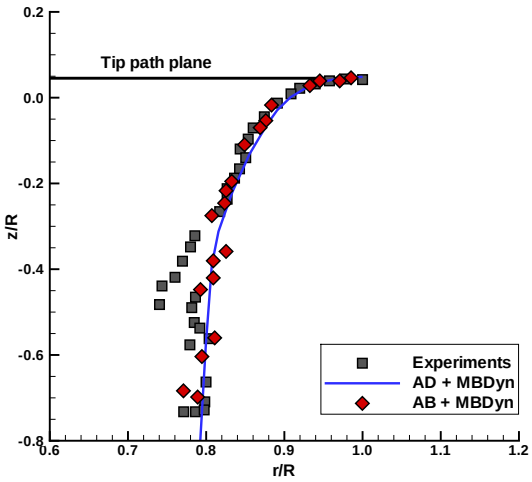

Figure 14: Tip vortex core displacements: comparison between PIV [11] data and CFD results.

The velocity distribution over the first cycle (0), that was computed by MBDyn using the Pitt-Peters [27] inflow model, is slightly different between the two cases because of the interpolation performed by ROSITA over different grids.

An example of the evolution of the MBDyn/ROSITA coupling cycles using the AB model is presented in Figure 12 where the instantaneous flow fields extracted from the final time step of each run are illustrated on a azimuthal plane at the same blade phase ($\psi = 0°$) by means of the vorticity magnitude contours. The spatial location of the blade tip vortex and its intensity reached a converged state after five iterations (cycle 4). The comparison between the final flow field solution (after 7 coupling cycles) and PIV measurements shows that the tip vortex core intensity is slightly underestimated by the CFD solver ROSITA. Nevertheless, both the tip vortex core trajectory and the velocity profiles in the rotor slipstream are well predicted by ROSITA, as respectively shown in Figure 14 and 15. The very good agreement between numerical results and experimental data demonstrated the trimmed AB model proposed in this paper is able to correctly reproduce the rotor wake structure, the unsteady effects induced by the blade rotation and the rotor kinematics and performance.

6. CONCLUSIONS

In this work an effective modelling approach has been presented to predict the unsteady, time-accurate flow field around helicopter rotors. Using this approach it is possible to get rid of the development of complex body-conformal grids. This leads to a significant reduction of the problem set-up time. Differently from the approach followed by other authors, the identification of the position of the source term to be inserted is developed exploiting the capability of overset moving grids. This leads to computational times which are clearly higher than those required by the actuator disk model, but that are still competitive when compared to those required by model based on detailed near body grids. Significant reductions of the computational time is achieved since the overall grid size is strongly reduced with respect to detailed blade representations. Moreover, convergence properties of the computations are improved since rotating blades are replaced by sources distributions and thus solid walls boundary conditions are not needed. Very simple modifications to the overset grid management may allow further computational savings in the future.

The comparison of the simulation performed with experimental results of a tiltrotor in hover allowed to show a very good agreement of the prediction of the tip vortex trajectory. The comparison of the instantaneous velocity field computed using the the actuator disk with the one obtained with the actuator blade, allowed to show how the time accurate model of the actuator blade correctly predicts the effect of the blade passage in the induced velocity field.

This effect can be very important when it is necessary to identify the interference loads developed by the rotor blades on other bodies, e.g. the fuselage of an helicopter or the wing of a tiltrotor, or the interference between coaxial rotors. In fact, the employment of this approach may lead to more accurate identification of inflow velocity models.

References

[1] Chuiton, F. L., "Actuator Disc Modelling for Helicopter Rotors," *Aerospace Science and Technology*, Vol. 8, 2004, pp. 285–297.

[2] Whitfield, D. and Jameson, A., "Euler equation simulation of propeller-wing interaction in transonic flow," *Journal of Aircraft*, Vol. 21, No. 11, 1984, pp. 835–839.

[3] Chaffin, M. and Berry, J., "Helicopter fuselage aerodynamics under a rotor by Navier-Stokes simulation," *Journal of the American Helicopter Society*, Vol. 42, No. 3, 1997, pp. 235–242.

[4] O'Brien, D. and Smith, M., "Analysis of Rotor–Fuselage Interactions Using Various Rotor Mod-

els," 43^{th} *AIAA Aerospace Science Meeting*, 2005, AIAA-2005-468.

[5] Fejtek, L. and Roberts, L., "Navier-Stokes Computation of Wing/Rotor Interaction for a Tilt Rotor in Hover," 29^{th} *AIAA Aerospace Science Meeting*, January 1991, AIAA 91-0707.

[6] Lynch, C., Prosser, D., and Smith, M., "An Efficient Actuating Blade Model for Unsteady Rotating System Wake Simulations," *Computers & Fluids*, Vol. 92, 2013, pp. 138–150.

[7] Biava, M., *RANS computations of rotor/fuselage unsteady interactional aerodynamics*, Ph.D. thesis, Politecnico di Milano, 2007.

[8] Masarati, P., Morandini, M., and Mantegazza, P., "An Efficient Formulation for General-Purpose Multibody/Multiphisics Analysis," *Journal of Computational and Nonlinear Dynamics*, Vol. 9, No. 4, pp. 041001.

[9] Biava, M., Valentini, M., and Vigevano, L., "Trimmed Actuator Disk Modeling for Helicopter Rotor," 39^{th} *European Rotorcraft Forum*, 3-6 September 2013.

[10] Droandi, G., *Wing–Rotor Aerodynamic Interaction in Tiltrotor Aircraft*, Ph.D. thesis, Politecnico di Milano, 2014.

[11] Droandi, G., Zanotti, A., Gibertini, G., Grassi, D., and Campanardi, G., "Experimental Investigation of the Rotor-Wing Aerodynamic Interaction in a Tiltwing Aircraft in Hover," *The Aeronautical Journal*, Vol. 119, No. 1215, May 2015, pp. 591–612.

[12] Spalart, P. and Allmaras, S., "One equation model for aerodynamic flows," 30^{th} *AIAA Aerospace Science Meeting & Exhibit*, 1992, AIAA 92-0439.

[13] Roe, P. L., "Approximate Riemann Solvers, Parameter Vectors and Difference Schemes," *Journal of Computational Physics*, Vol. 43, 1981, pp. 357–372.

[14] Venkatakrishnan, V., "On the accuracy of limiters and convergence to steady state solutions," 31^{st} *AIAA Aerospace Science Meeting & Exhibit*, 1993, AIAA 1993-880.

[15] Jameson, A., "Time Dependent Calculations Using Multigrid with Applications to Unsteady Flows past Airfoils and Wings," 10^{th} *AIAA Computational Fluid Dynamics Conference*, 1991, AIAA 91-1596.

[16] Chesshire, G. and Henshaw, W. D., "Composite overlapping meshes for the solution of partial differential equations," *Journal of Computational Physics*, Vol. 90, 1990, pp. 1–64.

[17] Masarati, P., Piatak, D. J., Quaranta, G., Singleton, J. D., and Shen, J., "Soft-Inplane Tiltrotor Aeromechanics Investigation Using Two Comprehensive Multibody Solvers," *Journal of the American Helicopter Society*, Vol. 53, No. 2, 2008, pp. 179–192.

[18] O'Brien, D., *Analysis Of Computational Modeling Techniques For Complete Rotorcraft Configurations*, Ph.D. thesis, Georia Institute of Technology, 2006.

[19] Yu, N., Samant, S., and Rubbert, P., "Flow Prediction for Propfan Configurations Using Euler Equations," 17^{th} *AIAA Fluid Dynamics, Plasma Dynamics and Laser Conference*, June 1984, AIAA 84-1645.

[20] Alli, P., Nannoni, F., and Cicalè, M., "ERICA: The european tiltrotor design and critical technology projects," *AIAA/ICAS International Air and Space Symposium and Exposition: The Next 100 Years*, 14-17 July 2005.

[21] Droandi, G., Zanotti, A., Gibertini, G., Campanardi, G., and Grassi, D., "Experimental Investigation on a 1/4 Scaled Model of an High-Performance Tiltwing Aircraft in Hover," American Helicopter Society 70^{th} Annual Forum, Montreal, Canada, 20-22 May 2014.

[22] Droandi and Gibertini, G., "Aerodynamic Blade Design With Multi-Objective Optimization For A Tiltrotor Aircraft," *Aircraft Engineering and Aerospace Technology*, Vol. 87, No. 1, 2015, pp. 19–29.

[23] Zanotti, A., Grassi, D., and Gibertini, G., "Experimental Investigation of a Trailing Edge L-shaped Tab on a Pitching Airfoil in Deep Dynamic Stall Conditions," *Proc of IMechE, Part G: Journal of Aerospace Engineering*, Vol. 228, No. 12, 2014, pp. 2371–2382.

[24] PIVTEC, "PIVview 2C version 3.0. User manual," www.pivtec.com, January 2009.

[25] E.Turkel, Radespiel, R., and Kroll, N., "Assessment of Preconditioning Methods for Multidimensional Aerodynamics," *Computer and Fluids*, Vol. 26, No. 6, 1997, pp. 613–634.

[26] Abbott, I. and Doenhoff, A. V., *Theory of Wing Sections, Including a Summary of Airfoil Data*, McGraw–Hill Book Co., Inc. (Reprinted by Dover Publications, 1959), 1949.

[27] Pitt, D. and Peters, D., "Theoretical Prediction of Dynamic-Inflow Derivatives," *Vertica*, Vol. 5, 1981, pp. 21–34.

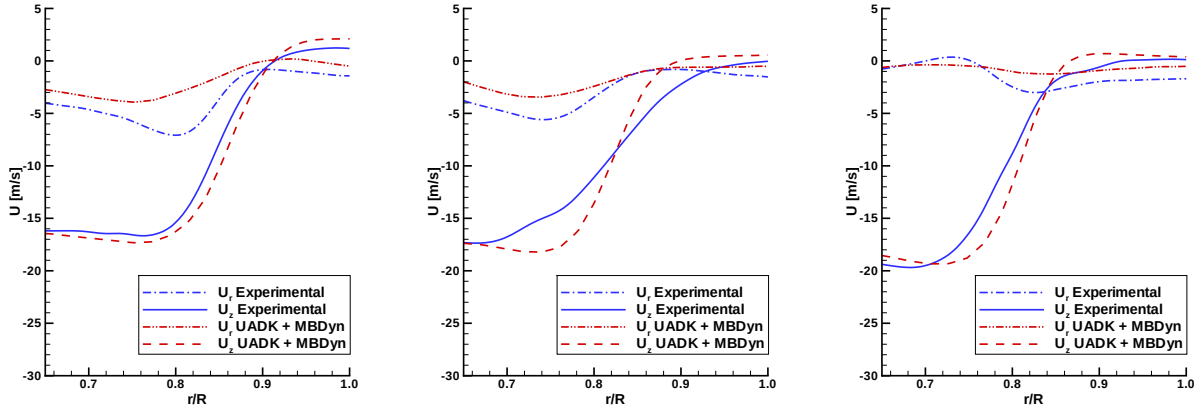

(a) $z/R = -0.15$ (b) $z/R = -0.33$ (c) $z/R = -0.50$

Figure 15: Radial distribution of U_r and U_z velocity components extracted ad different vertical positions ($\psi = 45°$): comparision between PIV measurements [11] and unsteady CFD calculations extracted from the final time step of the final coupling iteration (cycle 6).